Supporting Information for

Cyclic Square Wave Voltammetry of Surface-Confined Quasireversible Electron Transfer Reactions

*Megan A. Mann and Lawrence A. Bottomley**

School of Chemistry and Biochemistry, Georgia Institute of Technology, Atlanta, GA

30332-0400

AUTHOR EMAIL ADDRESS: Bottomley@gatech.edu

Table of Contents

Note: Plotting convention used for all figures in the supporting information is used: open circles denote specific parameter levels for simulated data; closed circles denote specific parameter levels for experimental data.

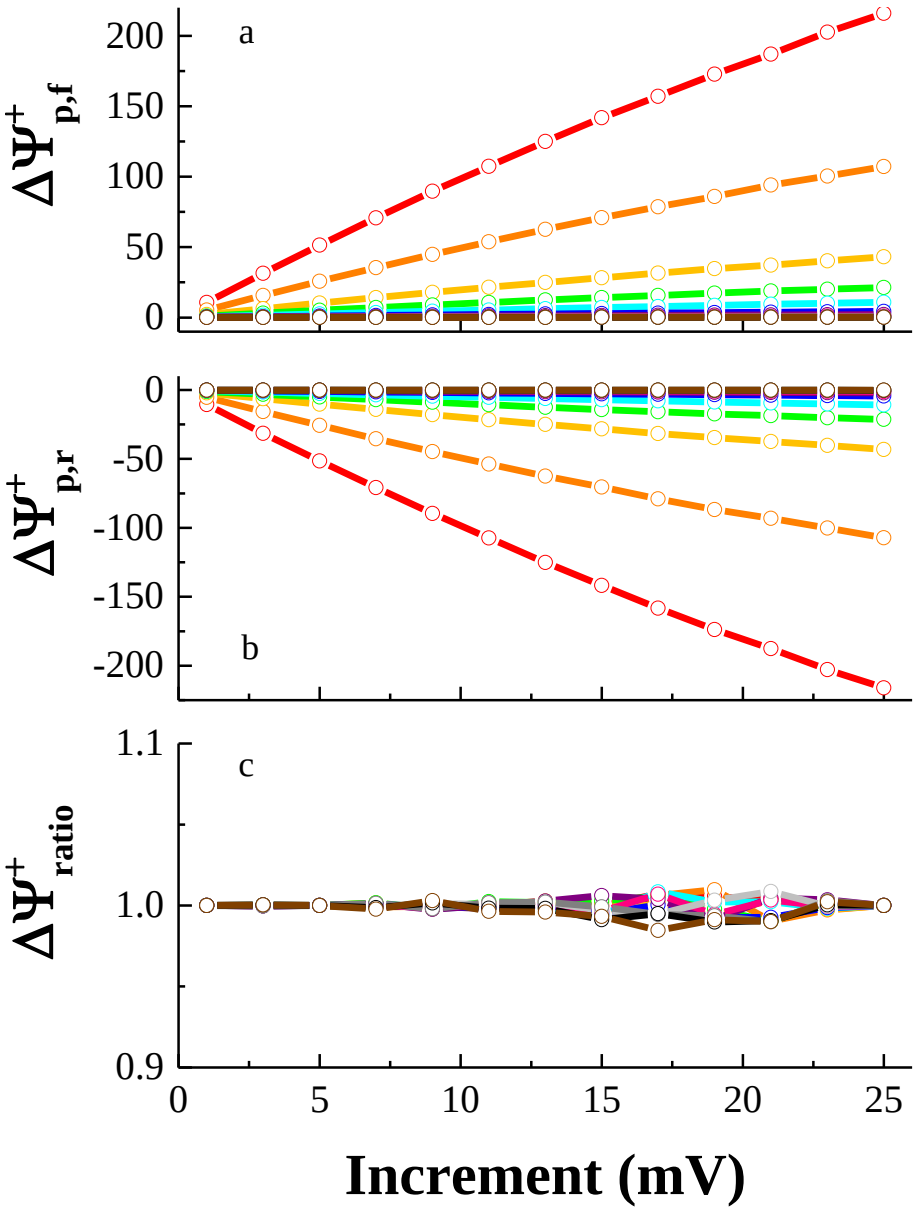

Figure S-1. The dependence of net peak current on increment: a) $\Delta\Psi^{s}_{p,f}$, b) $\Delta\Psi^{s}_{p,r}$, and c) peak ratio when $\alpha = 0.5$, amplitude = 50 mV, $\log k^0 = -1$, and period = 1 ms (red), 2 ms (orange), 5 ms (gold), 10 ms (green), 20 ms (cyan), 50 ms (blue), 100 ms (purple), 200 ms (magenta), 500 ms (light gray), 1 s (gray), 2 s (black), and 5 s (brown).

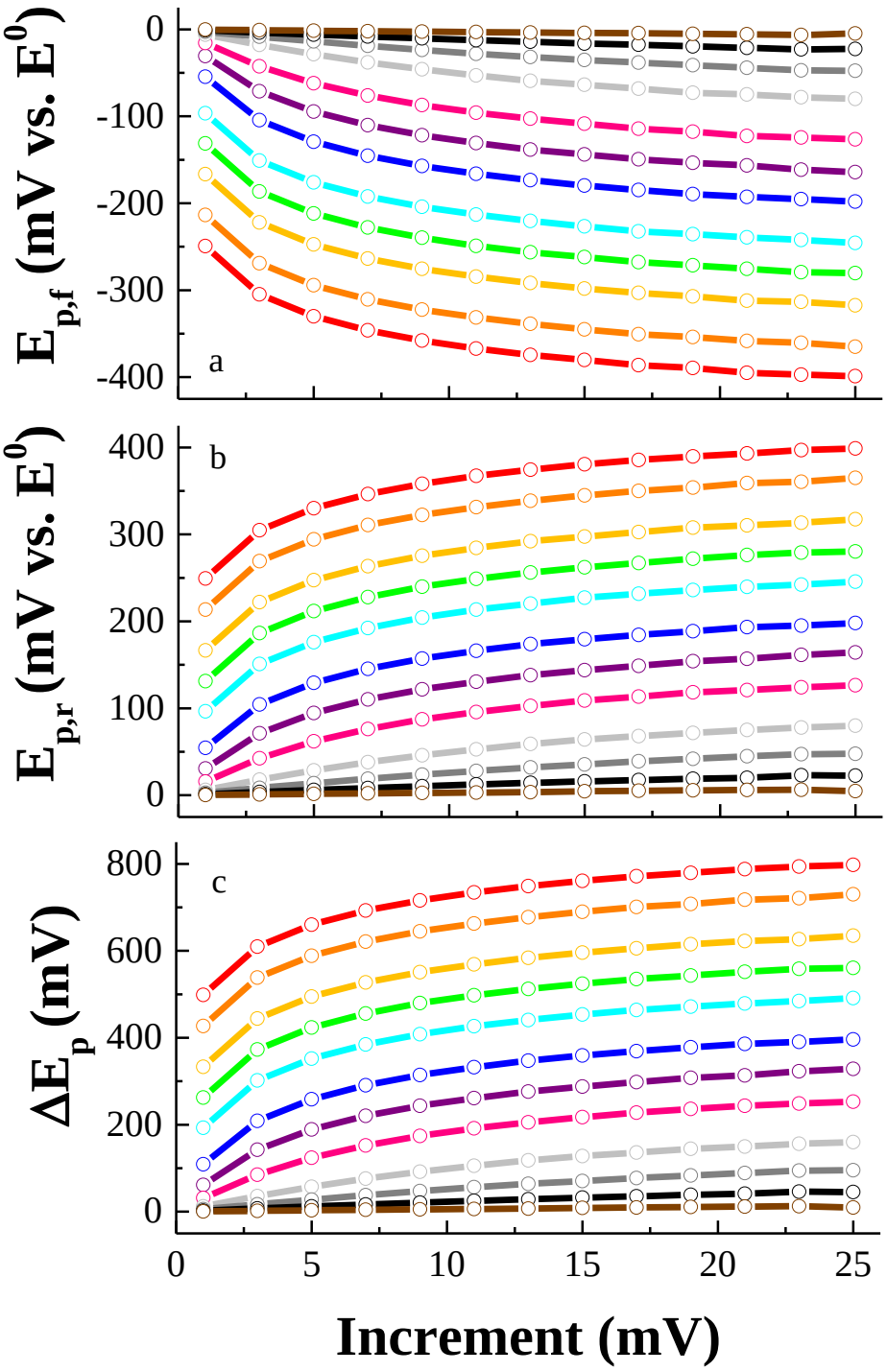

Figure S-2. The dependence of peak potential on increment: a) $E_{p,f}$, b) $E_{p,r}$, and c) ΔE_p when α = 0.5, amplitude = 50 mV, log k^0 = -1, and period = 1 ms (red), 2 ms (orange), 5 ms (gold), 10 ms (green), 20 ms (cyan), 50 ms (blue), 100 ms (purple), 200 ms (magenta), 500 ms (light gray), 1 s (gray), 2 s (black), and 5 s (brown).

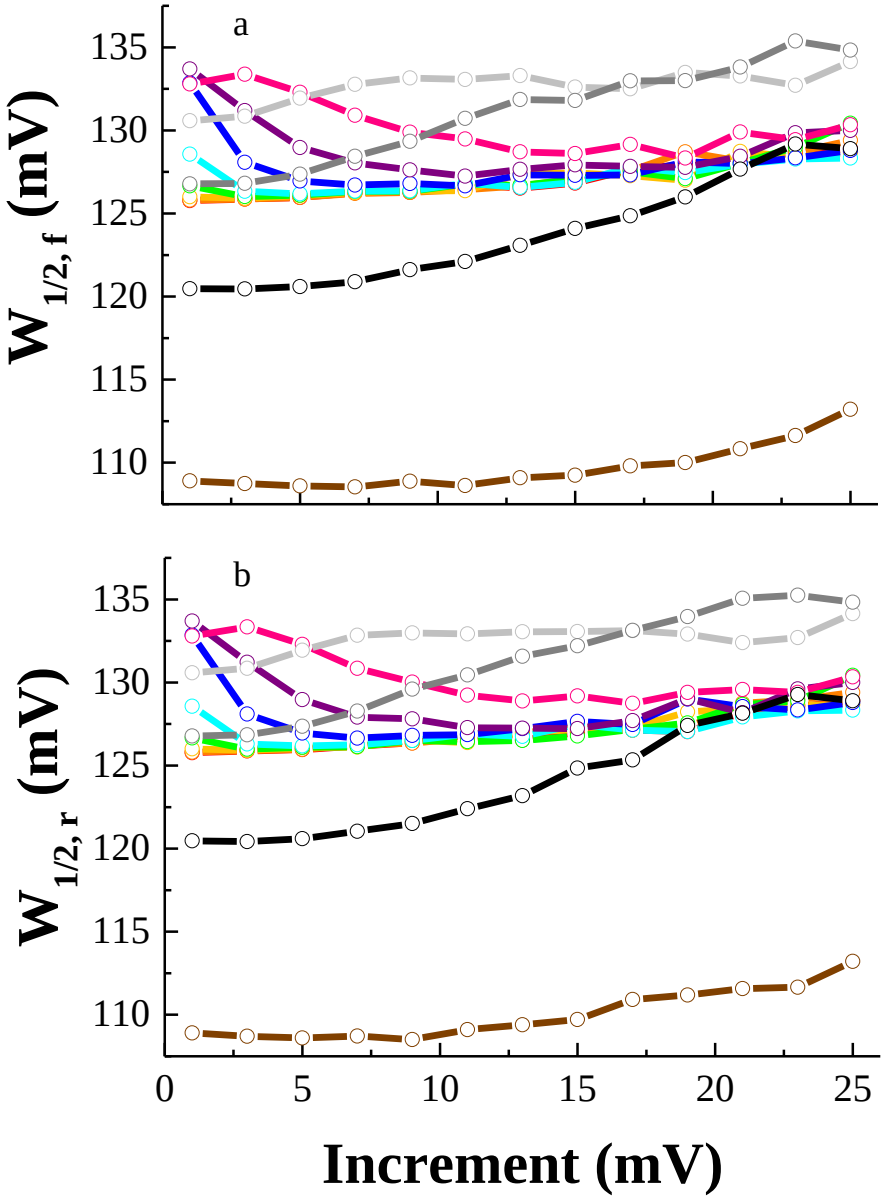

Figure S-3. The dependence of peak width on increment: a) $W_{1/2,f}$ and b) $W_{1/2,r}$ when $\alpha = 0.5$, amplitude = 50 mV, $\log k^0 = -1$, period = 1 ms (red), 2 ms (orange), 5 ms (gold), 10 ms (green), 20 ms (cyan), 50 ms (blue), 100 ms (purple), 200 ms (magenta), 500 ms (light gray), 1 s (gray), 2 s (black), and 5 s (brown).

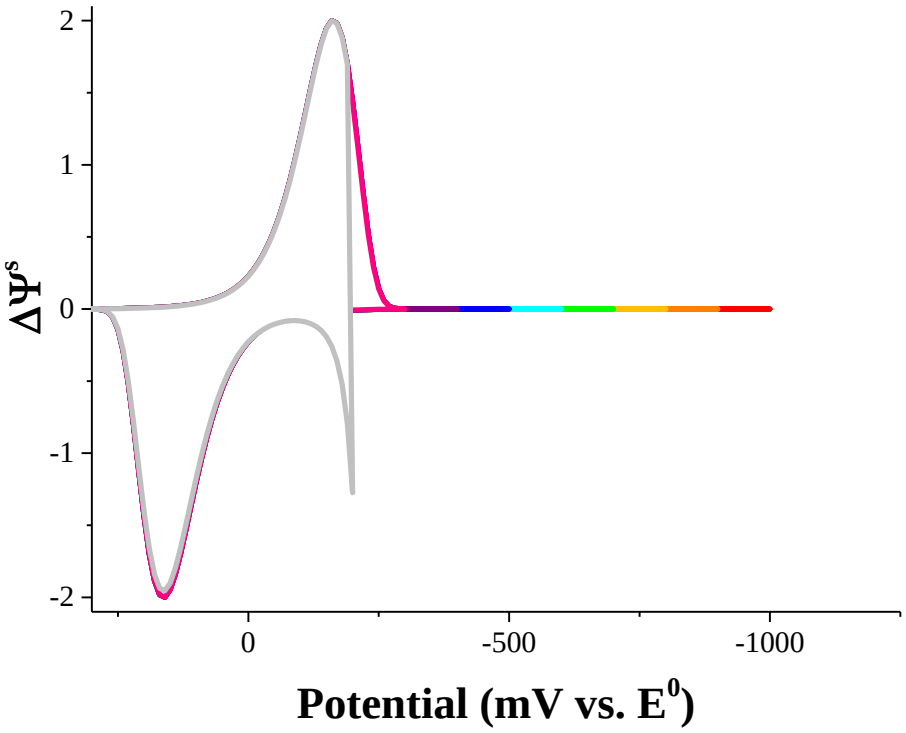

Figure S-4. The effect of switching potential on the shape of the voltammogram when log k^0 = -1, α = 0.5, amplitude = 50 mV, increment = 10 mV, period = 50 ms, and the switching potential was varied from 200 (light gray) to 1000 (red) mV negative of E^0 in 100 mV steps.

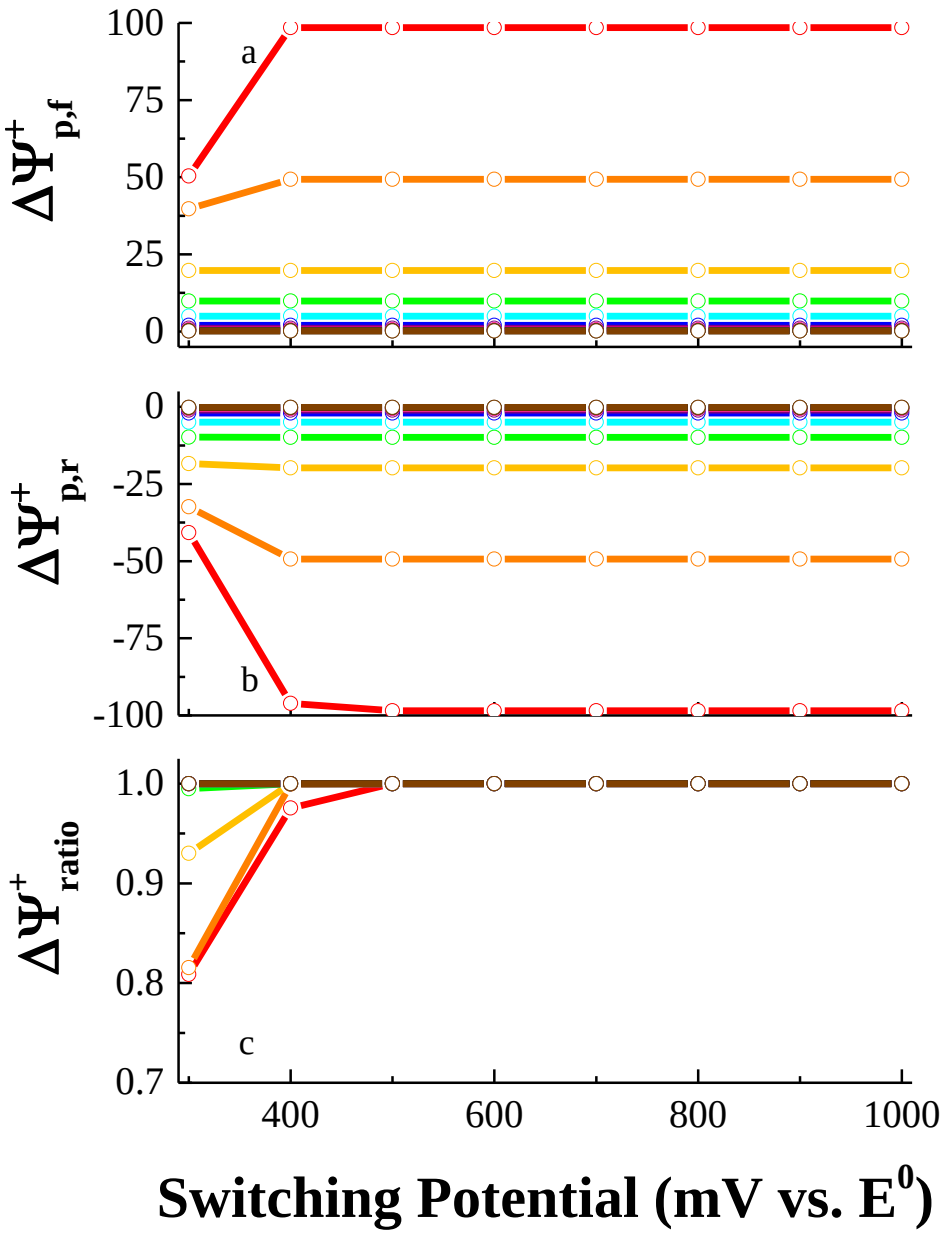

Figure S-5. The dependence of net peak current on switching potential: a) $\Delta\Psi^{s}_{p,f}$, b) $\Delta\Psi^{s}_{p,r}$, and c) peak ratio when $\alpha = 0.5$, amplitude = 50 mV, increment = 10 mV, log k^0 = -1, and period = 1 ms (red), 2 ms (orange), 5 ms (gold), 10 ms (green), 20 ms (cyan), 50 ms (blue), 100 ms (purple), 200 ms (magenta), 500 ms (light gray), 1 s (gray), 2 s (black), and 5 s (brown).

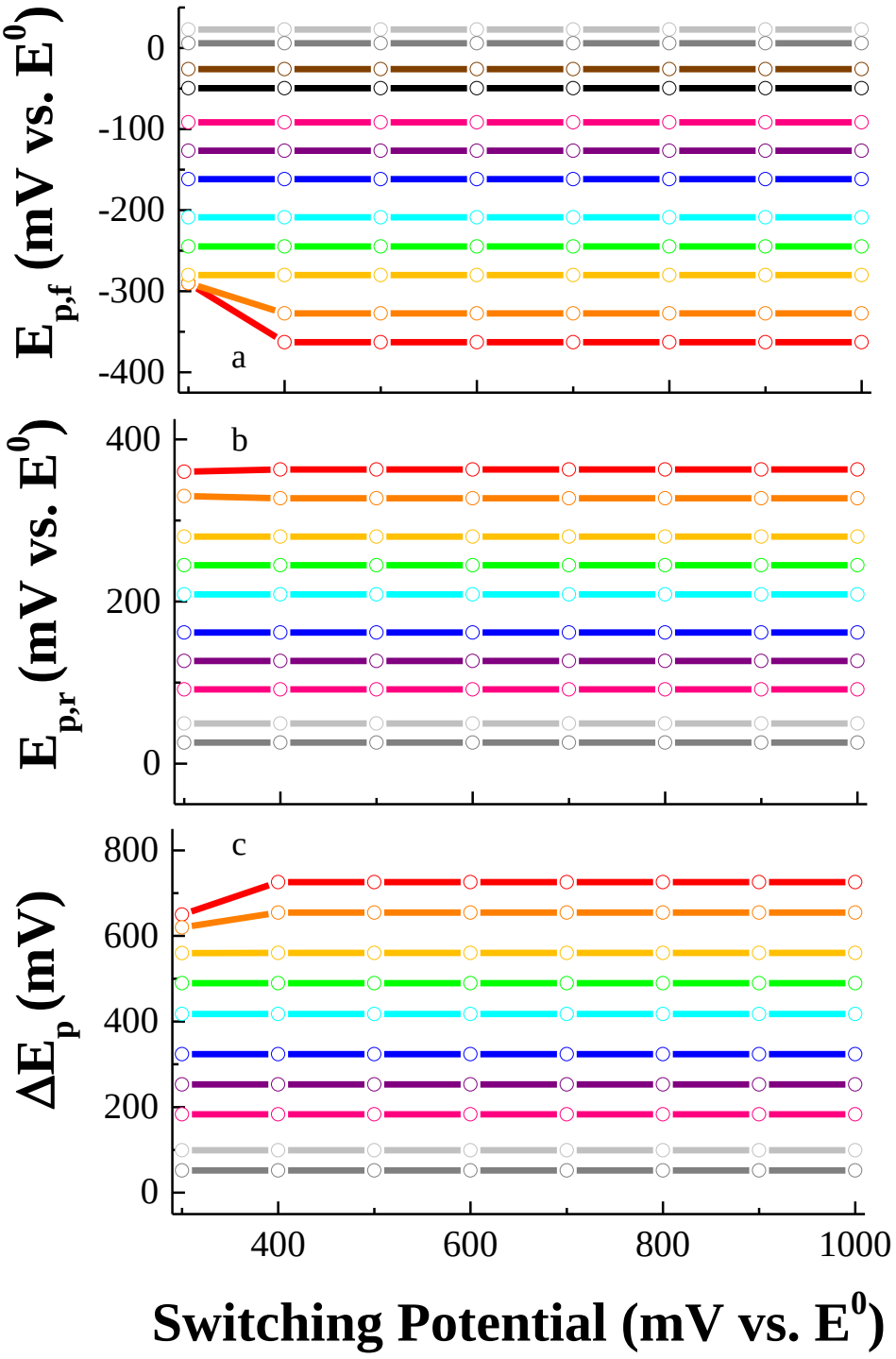

Figure S-6. The dependence of peak potential on switching potential: a) $E_{p,f}$, b) $E_{p,r}$, and c) ΔE_p when $\alpha = 0.5$, amplitude = 50 mV, increment = 10 mV, log $k^0 = -1$, and period = 1 ms (red), 2 ms (orange), 5 ms (gold), 10 ms (green), 20 ms (cyan), 50 ms (blue), 100 ms (purple), 200 ms (magenta), 500 ms (light gray), 1 s (gray), 2 s (black), and 5 s (brown).

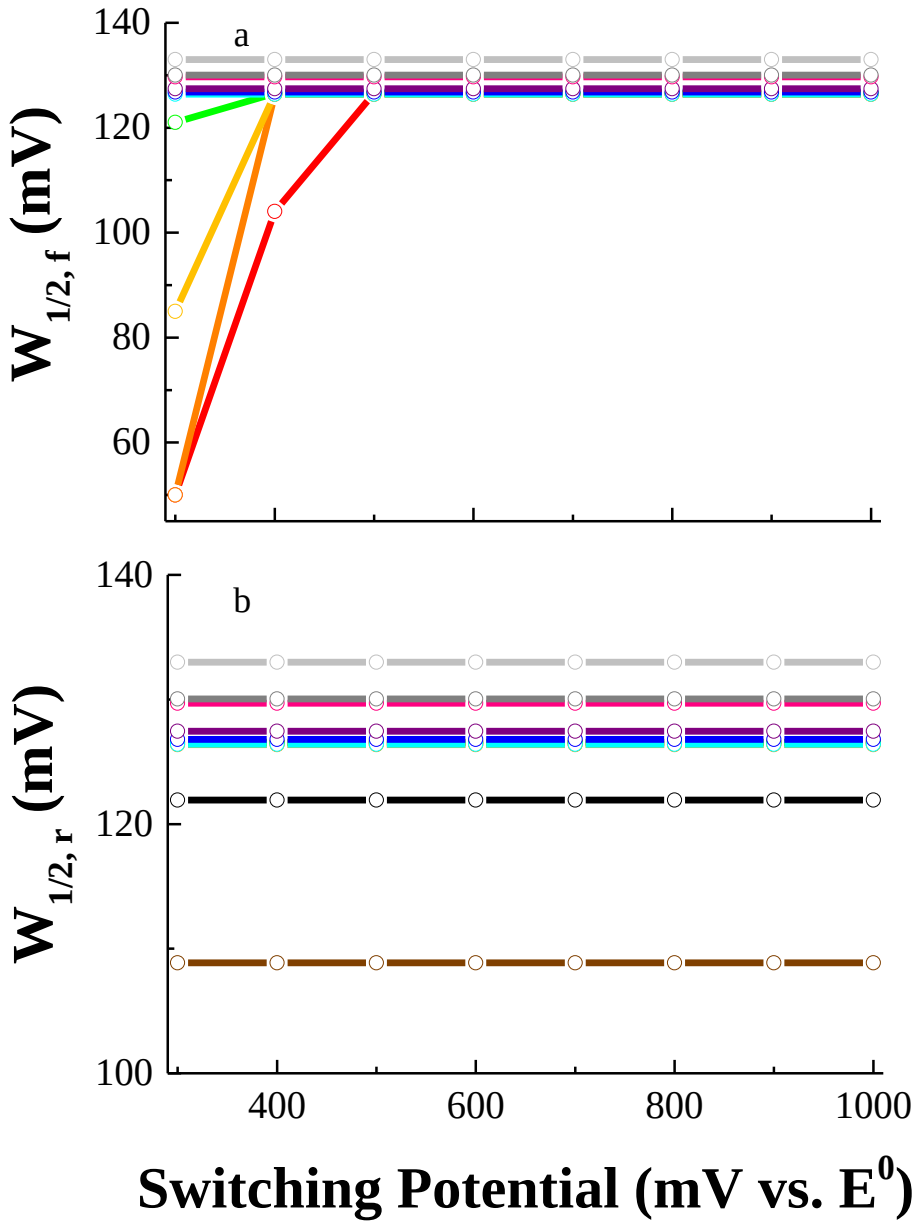

Figure S-7. The dependence of peak width on switching potential: a) $W_{1/2,f}$ and b) $W_{1/2,r}$ when α = 0.5, amplitude = 50 mV, increment = 10 mV, log k^0 = -1, and period = 1 ms (red), 2 ms (orange), 5 ms (gold), 10 ms (green), 20 ms (cyan), 50 ms (blue), 100 ms (purple), 200 ms (magenta), 500 ms (light gray), 1 s (gray), 2 s (black), and 5 s (brown).

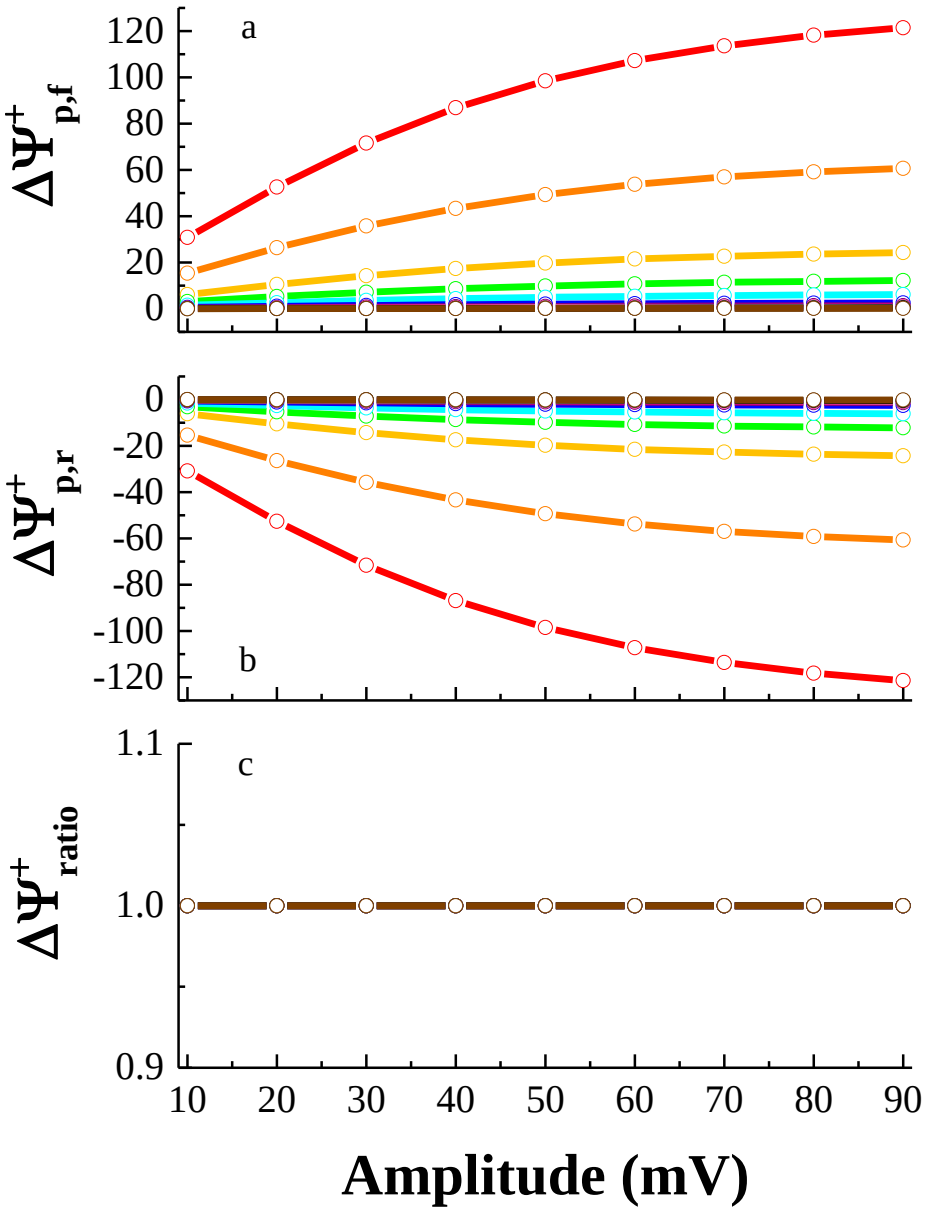

Figure S-8. The dependence of net peak current on amplitude: a) $\Delta\Psi^{s}_{p,f}$, b) $\Delta\Psi^{s}_{p,r}$, and c) peak ratio when $\alpha = 0.5$, increment = 10 mV, $\log k^{0} = -1$, and period = 1 ms (red), 2 ms (orange), 5 ms (gold), 10 ms (green), 20 ms (cyan), 50 ms (blue), 100 ms (purple), 200 ms (magenta), 500 ms (light gray), 1 s (gray), 2 s (black), and 5 s (brown).

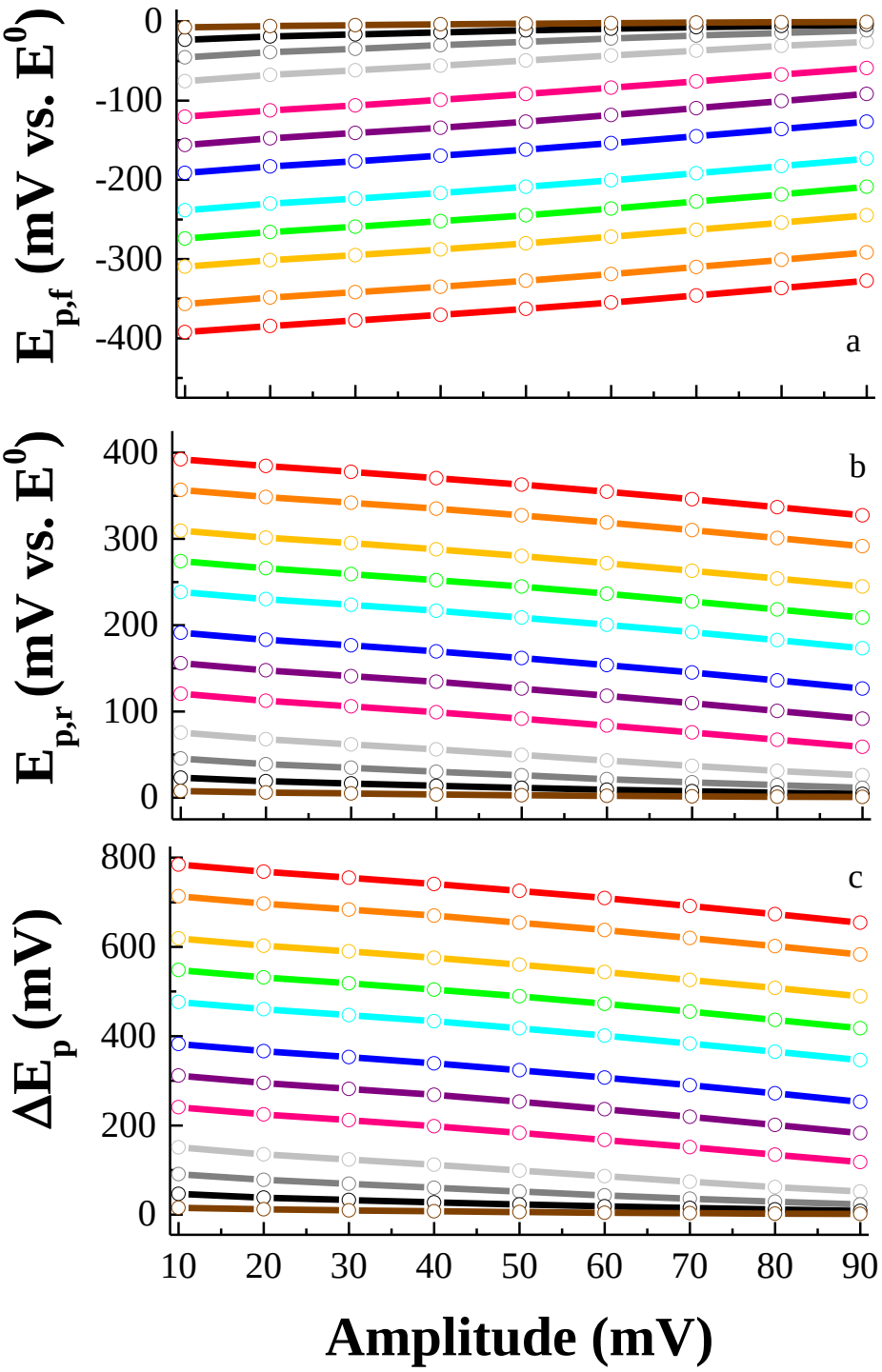

Figure S-9. The dependence of peak potential on amplitude: a) $E_{p,f}$, b) $E_{p,r}$, and c) ΔE_p when α = 0.5, increment = 10 mV, log k^0 = -1, and period = 1 ms (red), 2 ms (orange), 5 ms (gold), 10 ms (green), 20 ms (cyan), 50 ms (blue), 100 ms (purple), 200 ms (magenta), 500 ms (light gray), 1 s (gray), 2 s (black), and 5 s (brown).

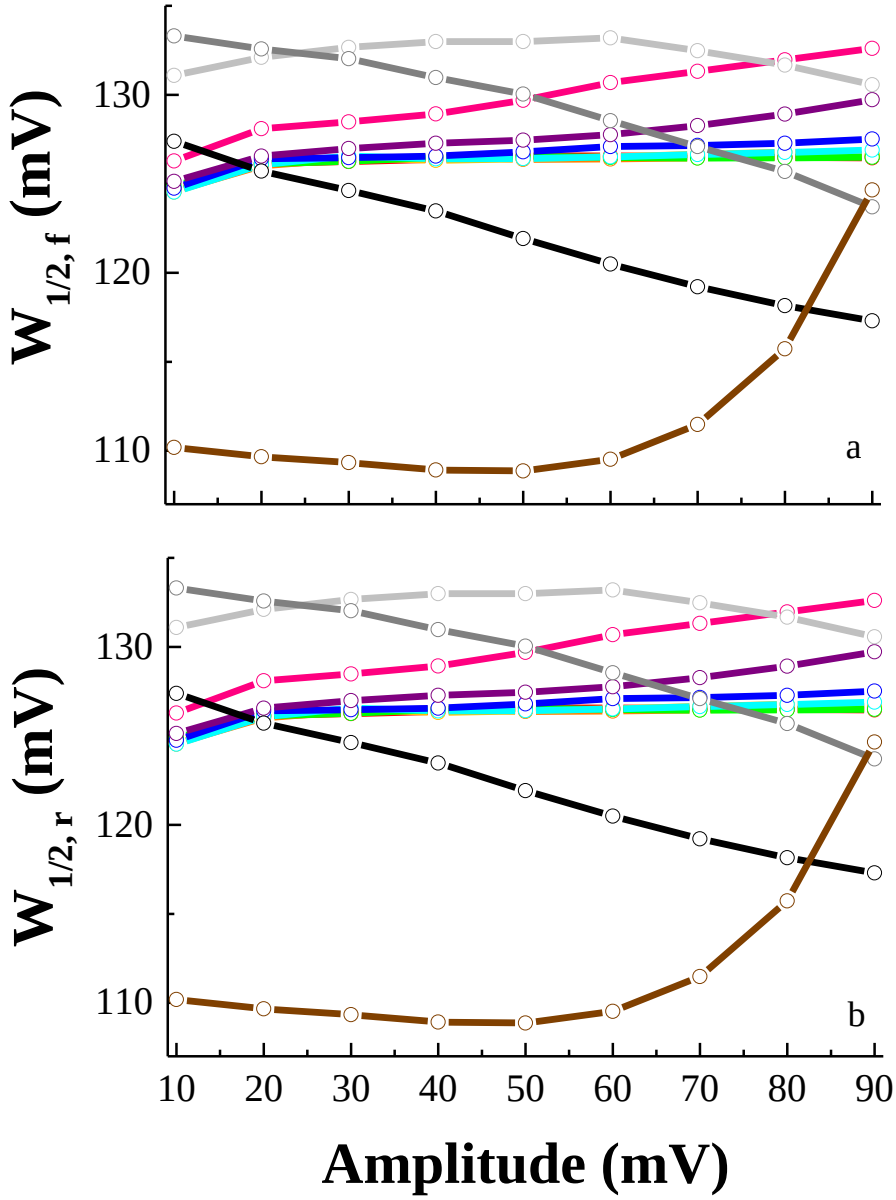

Figure S-10. The dependence of peak width on amplitude: a) $W_{1/2,f}$ and b) $W_{1/2,r}$ when $\alpha = 0.5$, increment = 10 mV, $\log k^0 = -1$, and period = 1 ms (red), 2 ms (orange), 5 ms (gold), 10 ms (green), 20 ms (cyan), 50 ms (blue), 100 ms (purple), 200 ms (magenta), 500 ms (light gray), 1 s (gray), 2 s (black), and 5 s (brown).

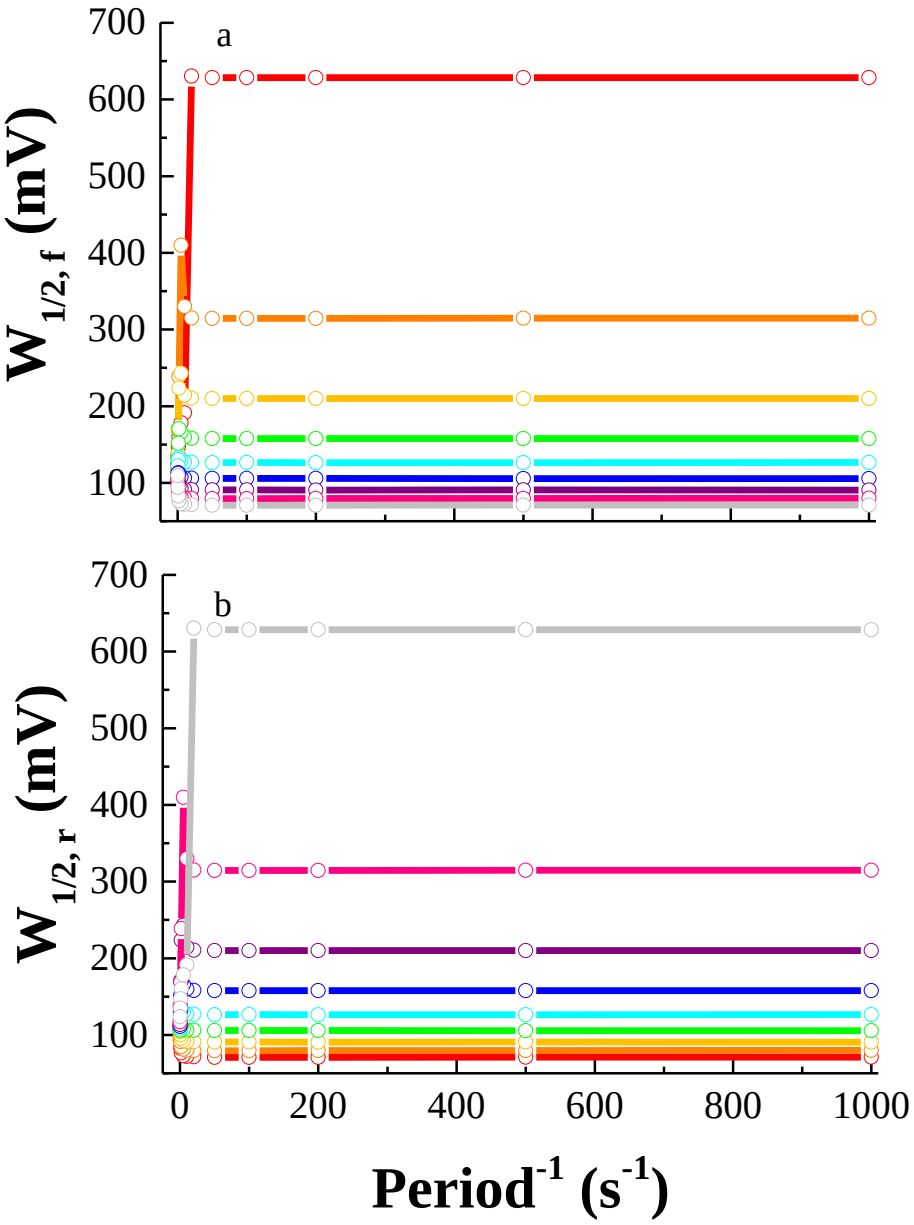

Figure S-11. The dependence of net peak current on period: a) $W_{1/2,f}$ and b) $W_{1/2,r}$ when amplitude = 50 mV, increment = 10 mV, log k^0 = -1, and α = 0.1 (red), 0.2 (orange), 0.3 (gold), 0.4 (green), 0.5 (cyan), 0.6 (blue), 0.7 (purple), 0.8 (magenta), and 0.9 (light gray).

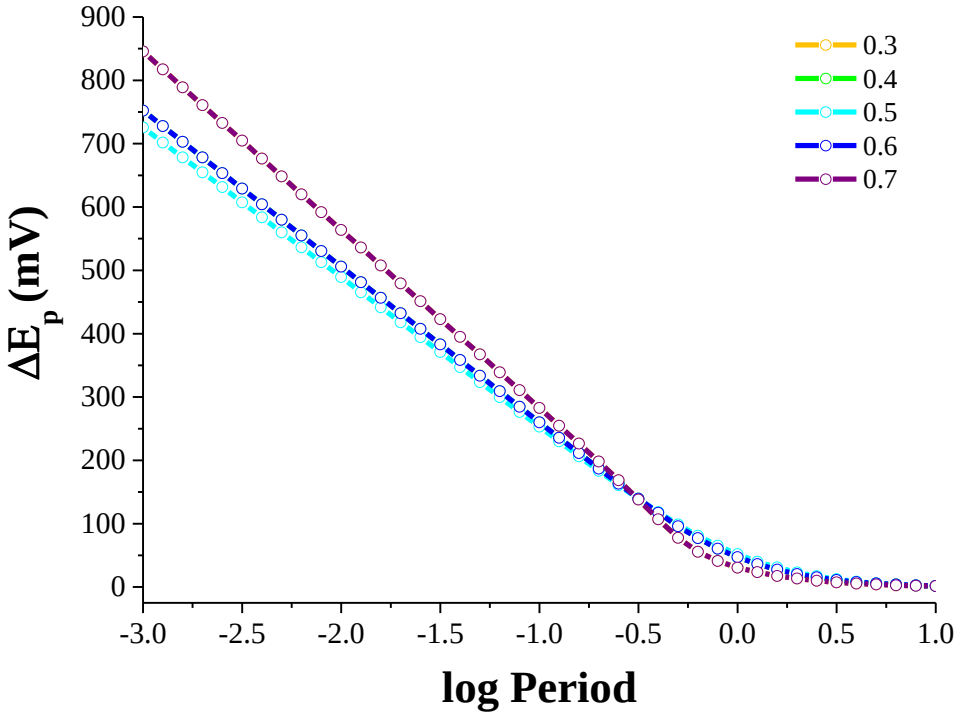

Figure S-12. Plot of peak separation versus log period as a function of α when log k^0 = -1, amplitude = 50 mV, increment = 10 mV, and where α is 0.3 (gold), 0.4 (green), , 0.5 (cyan), 0.6 (blue)and 0.7 (purple).

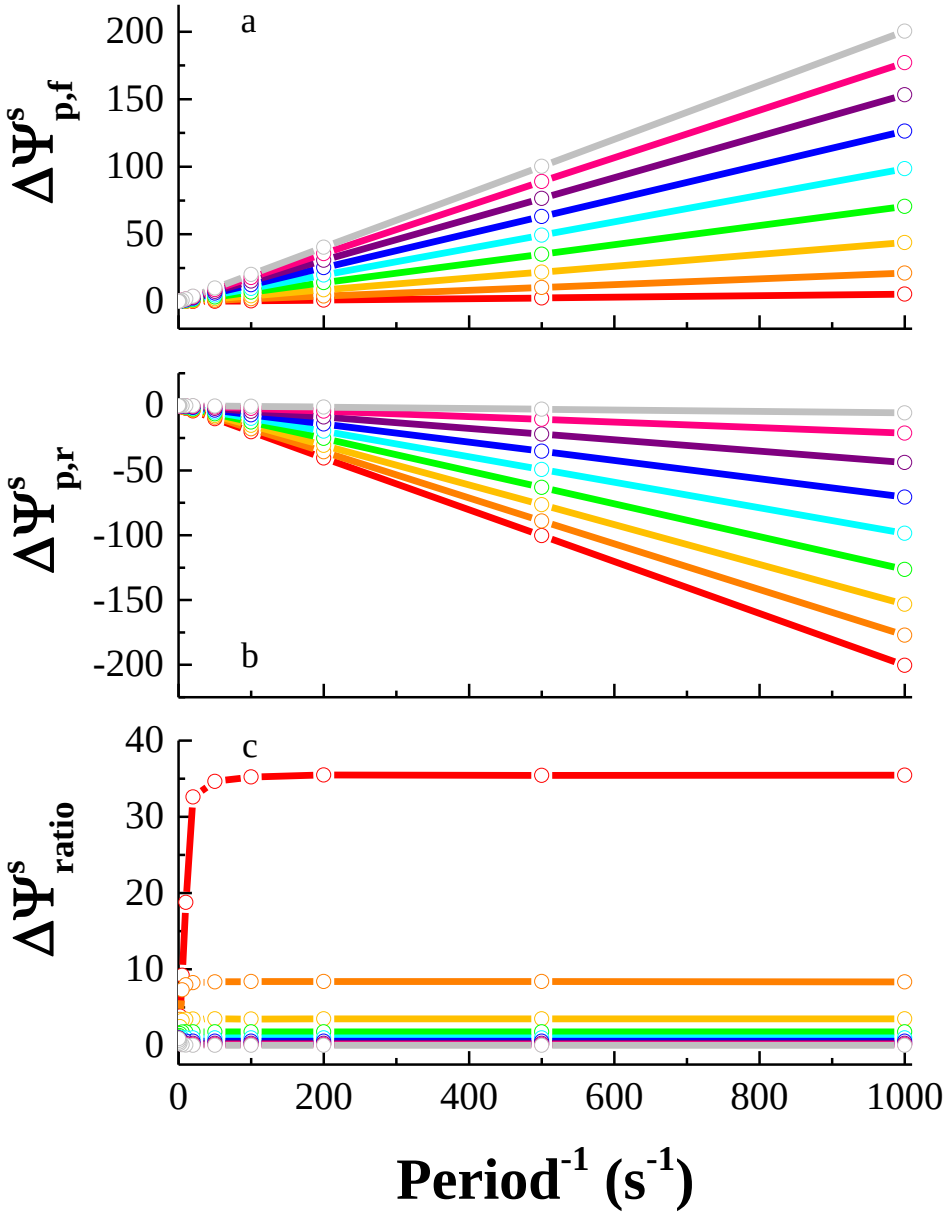

Figure S-13. The dependence of net peak current on period: a) $\Delta\Psi^s_{p,f}$, b) $\Delta\Psi^s_{p,r}$, and c) peak ratio when amplitude = 50 mV, increment = 10 mV, log k^0 = -1, and α = 0.1 (red), 0.2 (orange), 0.3 (gold), 0.4 (green), 0.5 (cyan), 0.6 (blue), 0.7 (purple), 0.8 (magenta), and 0.9 (light gray).

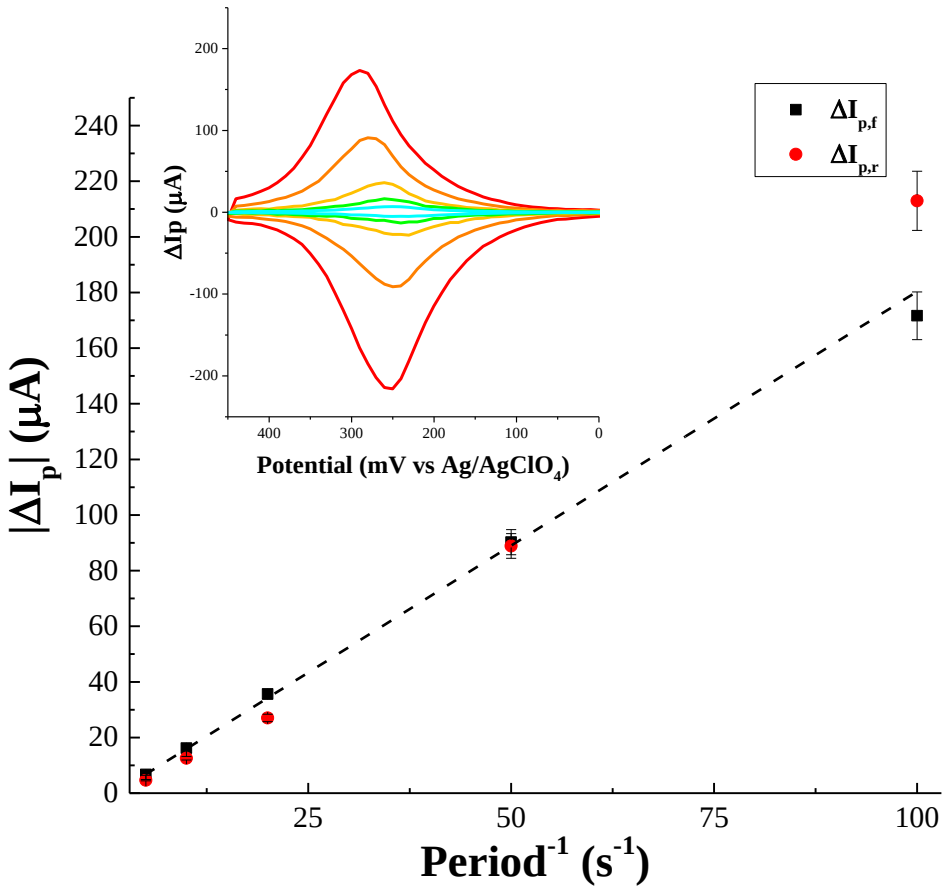

Figure S-14. Effect of period on ΔI_p for (Fc)CONH$(CH_2)_{15}$SH when amplitude = 20 mV, increment = 10 mV, and period is 10 (red) , 20 (orange), 50 (yellow), 100 (green), and 200 ms (cyan).

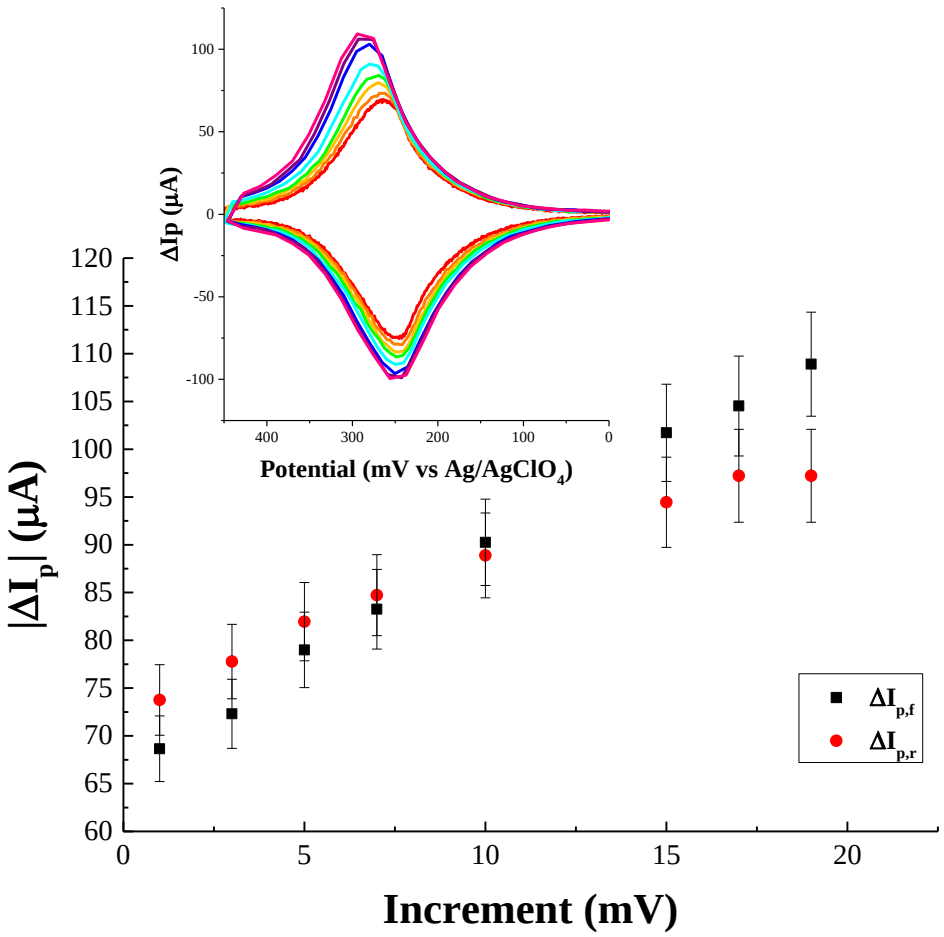

Figure S-15. Effect of increment on ΔI_p for (Fc)CONH$(CH_2)_{15}$SH when amplitude = 20 mV, period = 20 ms, and increment is 1 (red), 3 (orange), 5 (yellow), 7 (green), 10 (cyan), 15 (blue), 17 (purple), and 19 mV (pink).

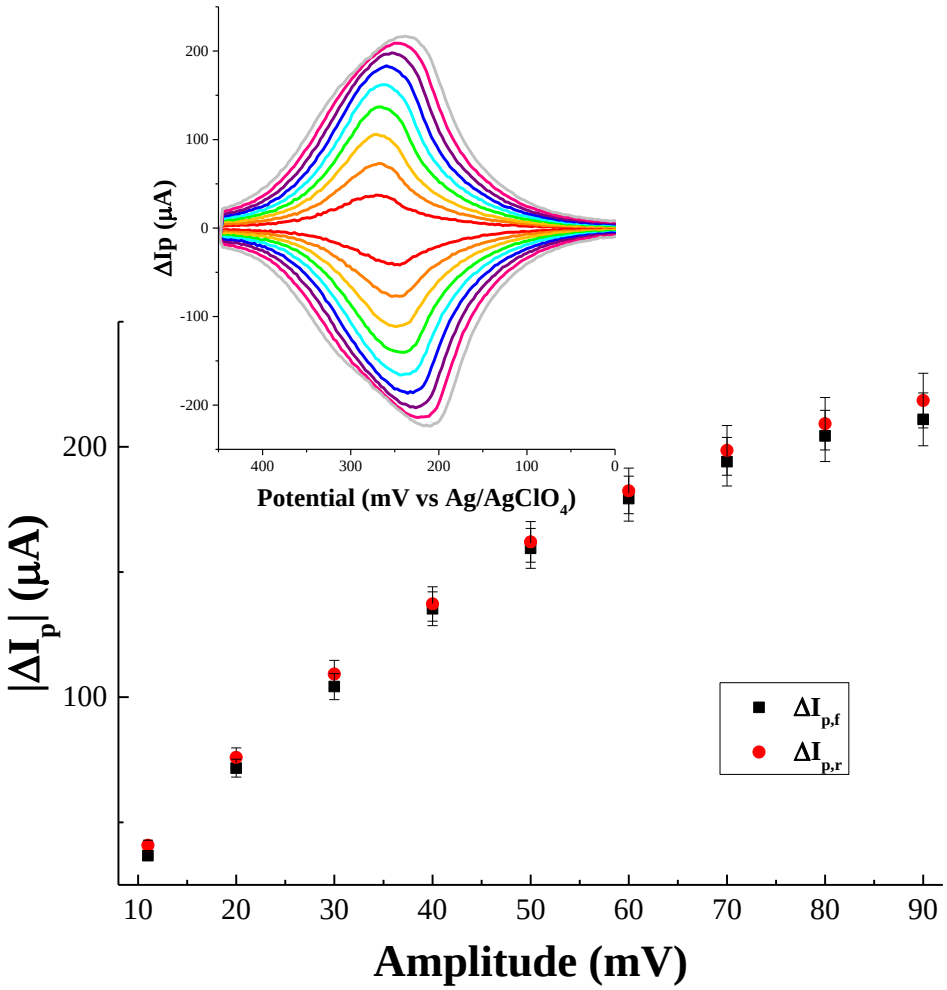

Figure S-16. Effect of amplitude on ΔI_p for (Fc)CONH$(CH_2)_{15}$SH when period = 20 ms, increment = 3 mV, and amplitude is varied from 10 (red) to 90 mV (light gray) in 10 mV steps.

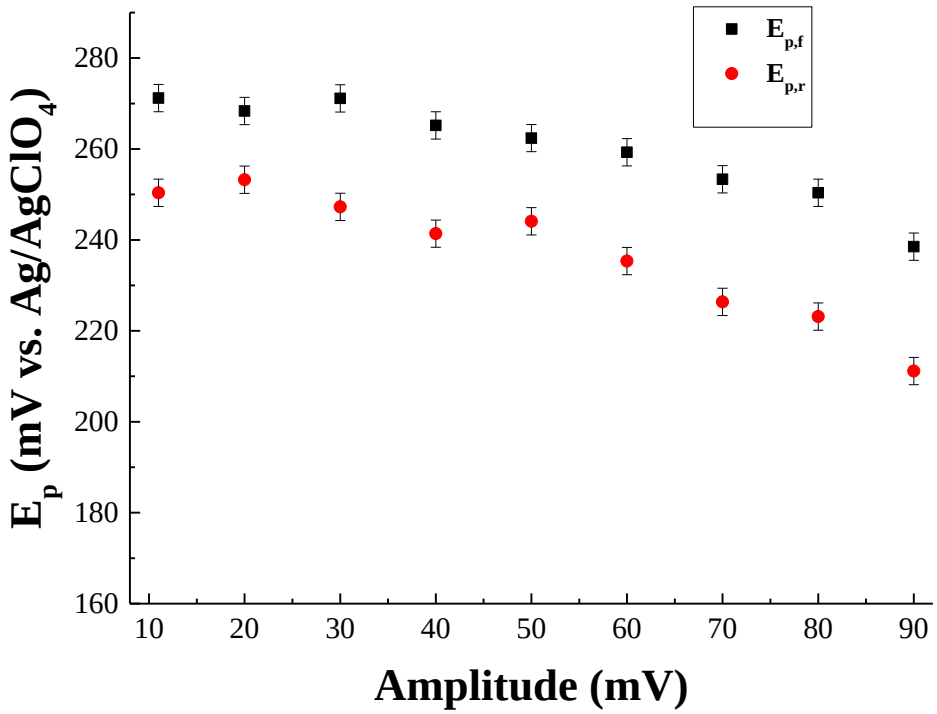

Figure S-17. Effect of amplitude on E_p for (Fc)CONH$(CH_2)_{15}$SH when when period = 20 ms, increment = 3 mV, and amplitude is varied from 10 to 90 mV in 10 mV steps.

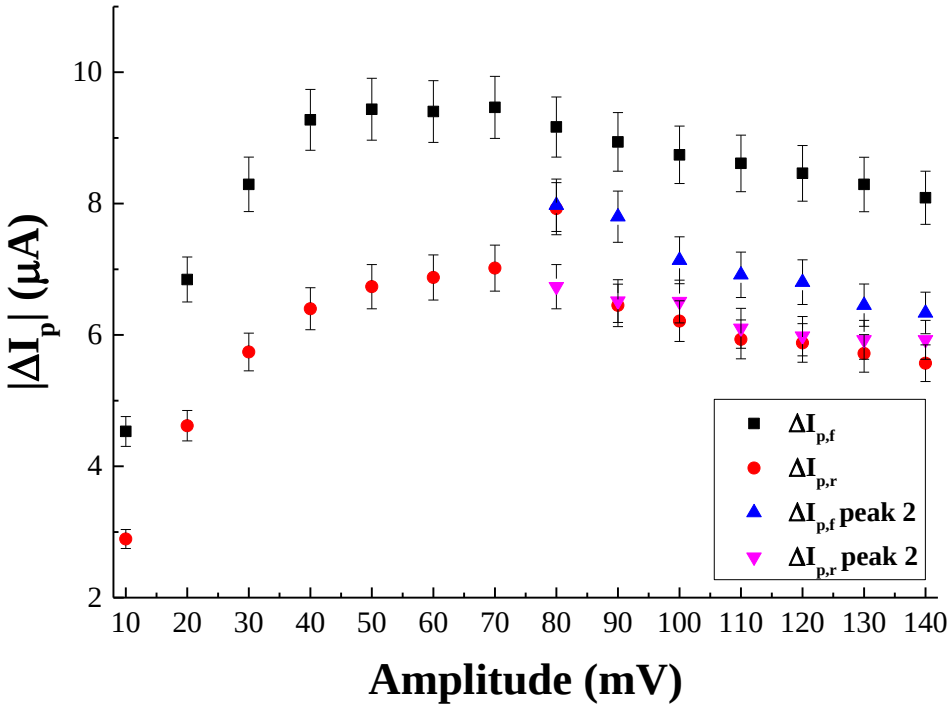

Figure S-18. Effect of amplitude on ΔI_p for (Fc)CONH$(CH_2)_{15}$SH when period = 200 ms, increment = 10 mV, and amplitude is varied from 10 to 140 mV in 10 mV steps.

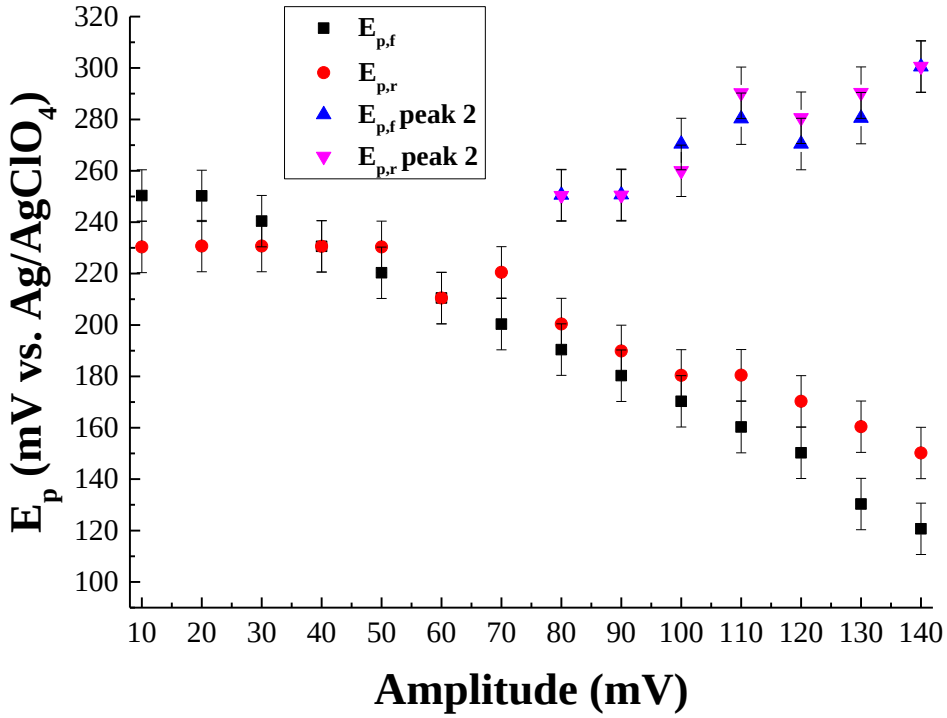

Figure S-19. Effect of amplitude on E_p for (Fc)CONH$(CH_2)_{15}$SH when when period = 200 ms, increment = 10 mV, and amplitude is varied from 10 to 140 mV in 10 mV steps.

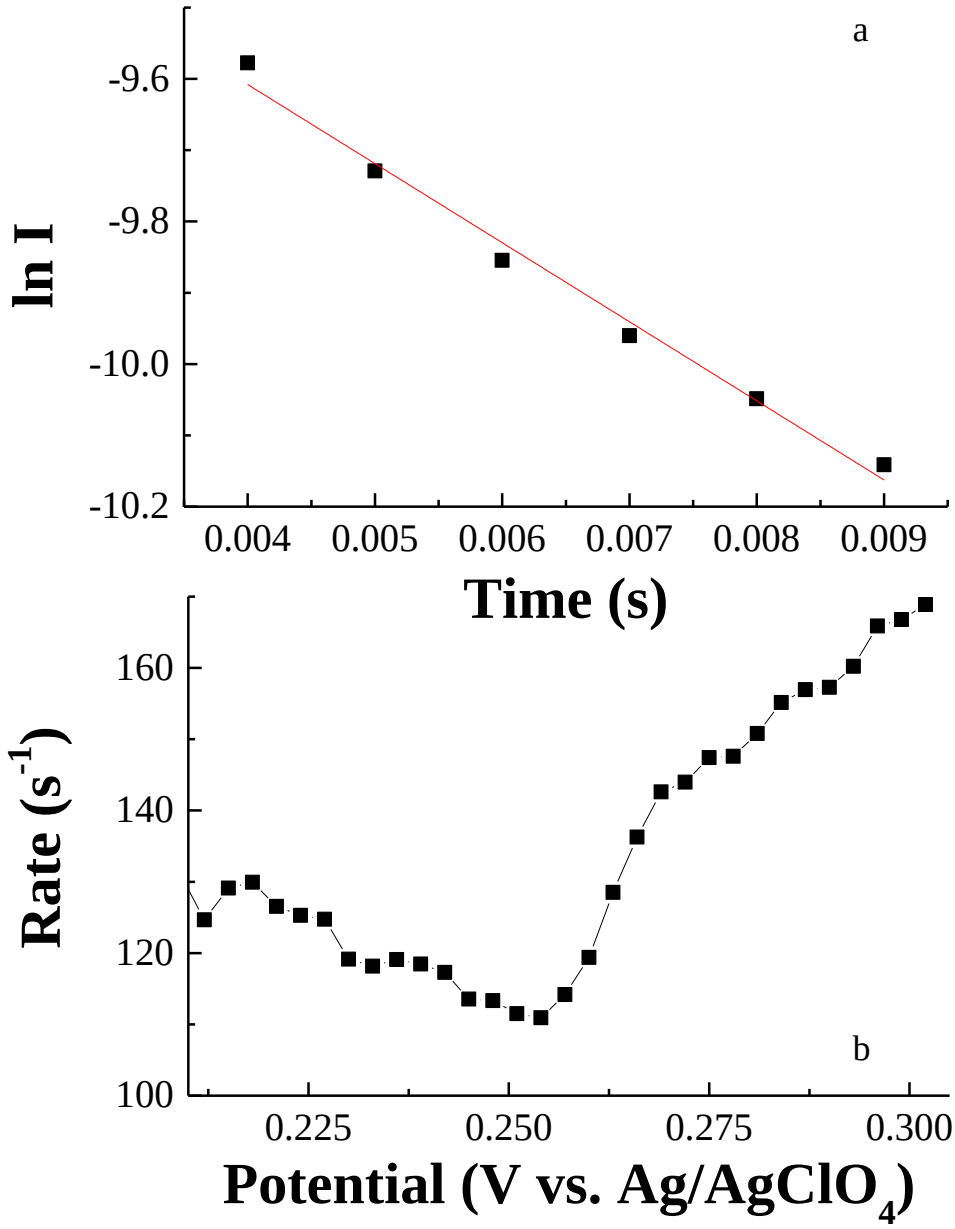

Figure S-20. The relationship between a) ln I and potential measured at E_{pulse} = 0.254 (V vs. $Ag/AgClO_4$) when amplitude = 20 mV, increment = 3 mV, and period = 20 ms where the slope of the best line of fit yields the rate and b) rate as a function of E_{pulse} for the same empirical parameters given in S-19a for $(Fc)CONH(CH_2)_{15}SH$.

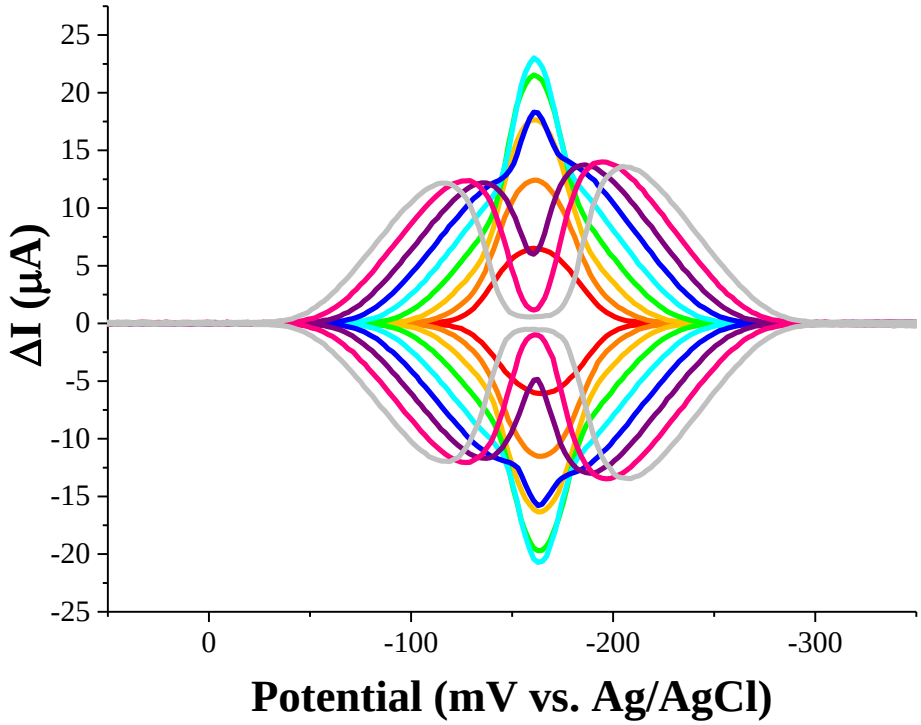

Figure S-21. The effect of amplitude on the AQDS experimental system when increment = 2 mV, period = 30 ms, and amplitude is varied from 10 (red) to 90 mV (gray) in 10 mV steps.

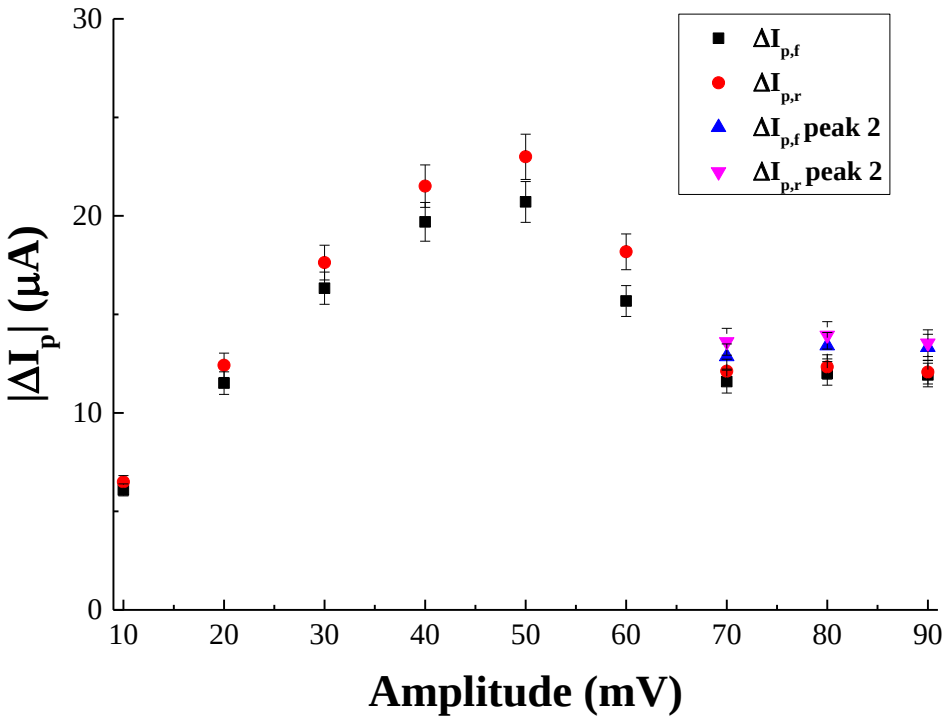

Figure S-22. The effect of amplitude on peak current for AQDS when period = 30 ms and increment = 2 mV.

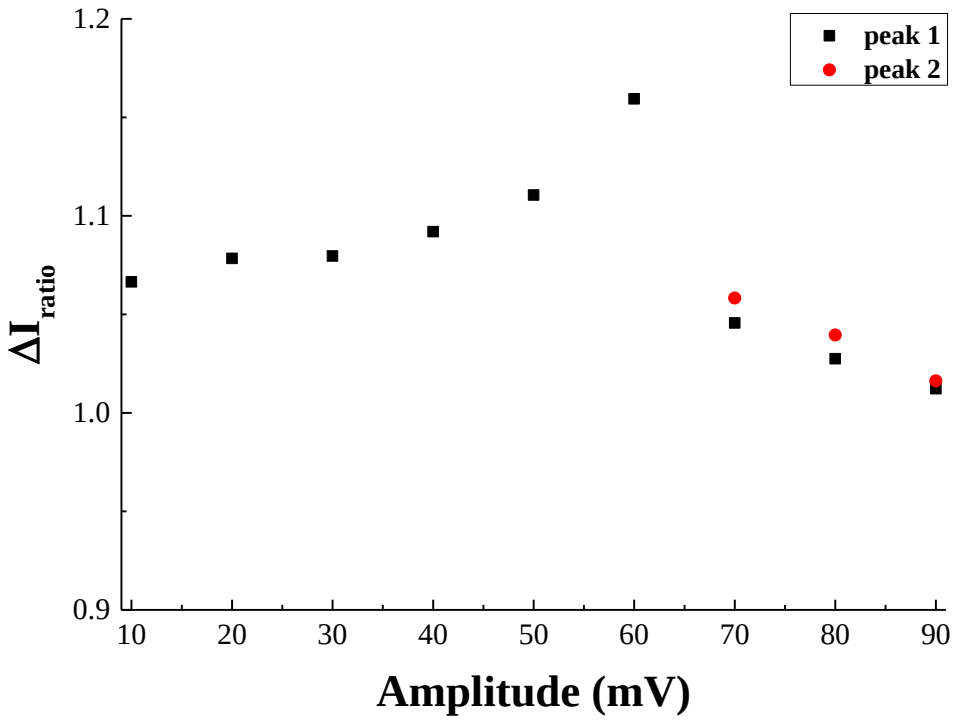

Figure S-23. The effect of amplitude on peak ratio for AQDS when period = 30 ms and increment = 2 mV.

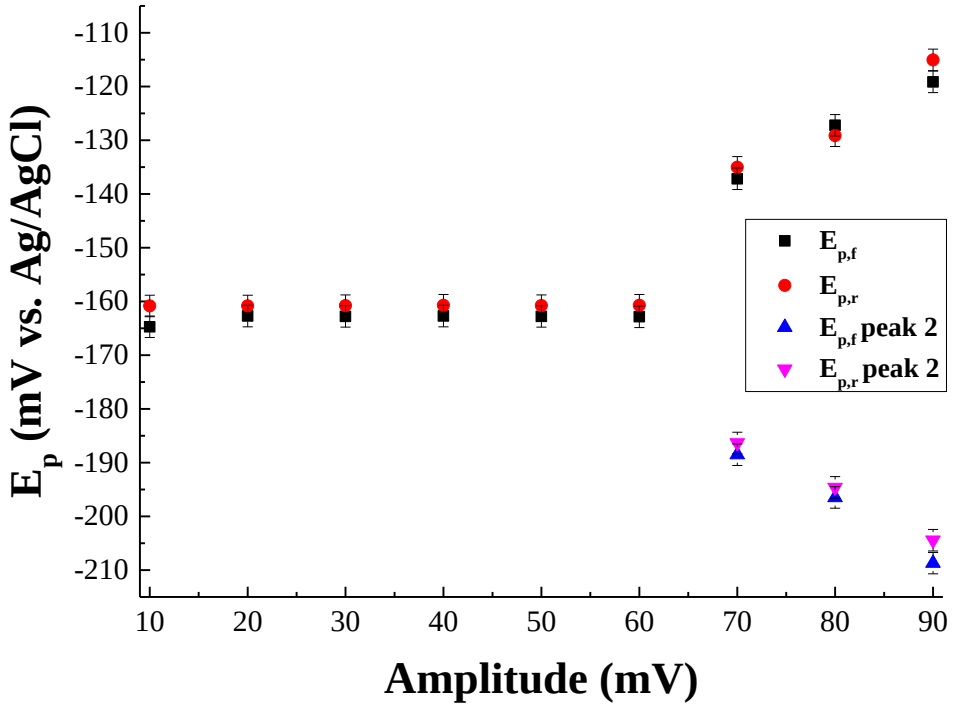

Figure S-24. The effect of amplitude on peak potential for AQDS when period = 30 ms and increment = 2 mV.

Derivation

The derivation of a dimensionless current equation from which theoretical voltammograms were computed is given below. Underlying assumptions in this derivation are that:

- no interactions exist between redox moieties on the electrode surface.
- the redox active adsorbate may be present as a either a single or multiple monolayers so long as no concentration gradient exists within the layers on the time scale of the voltammetric experiment.

The electrode reaction is:

$$Ox_{(ads)} + ne^- \rightleftharpoons Red_{(ads)} \quad (1)$$

At time t = 0, only $Ox_{(ads)}$ is present on the electrode surface.

$$\Gamma_{Ox} = \Gamma^*$$

$$\Gamma_{Red} = 0$$

This initial condition is also used by others.[1-5]

At time t > 0, $Ox_{(ads)}$ is converted to $Red_{(ads)}$, and the total surface concentration can be expressed as

$$\Gamma^* = \Gamma_{Ox} + \Gamma_{Red}$$

The amount of $Ox_{(ads)}$ converted to $Red_{(ads)}$ can be expressed by

$$\Gamma_{Red} = \int_0^t \frac{i(\tau)}{nFA}\, d\tau \quad (2)$$

The concentration of $Ox_{(ads)}$ at the electrode surface can be rewritten as

$$\Gamma_{Ox} = \Gamma^* - \Gamma_{Red} \quad (3)$$

$$\Gamma_{Ox} = \Gamma^* - \int_0^t \frac{i(\tau)}{nFA}\, d\tau \quad (4)$$

$$\text{Let } H = \frac{1}{nFA} \quad (5)$$

$$\text{and } I = \int_0^t i(\tau)d\tau \tag{6}$$

Using the Butler-Volmer equation for kinetics of electron transfer reactions

$$i = nFAk^0\left[\Gamma_{\text{Ox}}e^{-\alpha\phi} - \Gamma_{\text{Red}}e^{(1-\alpha)\phi}\right] \tag{7}$$

where $\phi = \frac{nF}{RT}\left(E^0 - E_{applied}\right)$, α is the transfer coefficient, n is the number of electrons transfer, F is the Faraday constant, k^0 is the electron transfer rate constant, and τ is the period.

By substitution, the Butler-Volmer relationship becomes

$$i = nFAk^0\left[\left(\Gamma^* - \text{HI}\right)e^{-\alpha\phi} - \text{HI}e^{(1-\alpha)\phi}\right] \tag{8}$$

To convert the current to a dimensionless current, the following transformation can be used

$$i(t) = \frac{nFA\Gamma^*}{\tau}\Psi(t) \tag{9}$$

Substituting the unitless current into the equation above

$$\Psi(t)\frac{nFA\Gamma^*}{\tau} = nFAk^0\left[\left(\Gamma^* - \Psi(t)\frac{\Gamma^*}{\tau}\right)e^{-\alpha\phi} - \Psi(t)\frac{\Gamma^*}{\tau}e^{(1-\alpha)\phi}\right] \tag{10}$$

Simplifying

$$\Psi(t) = \frac{k^0\tau}{\Gamma^*}\left[\left(\Gamma^* - \Psi(t)\frac{\Gamma^*}{\tau}\right)e^{-\alpha\varphi} - \Psi(t)\frac{\Gamma^*}{\tau}e^{(1-\alpha)\varphi}\right] \tag{11}$$

Further simplification

$$\Psi(t) = \left(k^0\tau - k^0\Psi(t)\right)e^{-\alpha\varphi} - k^0\Psi(t)e^{(1-\alpha)\varphi} \tag{12}$$

To solve the integrals in the dimensionless current, a numerical summation can be used by dividing each time step into subintervals. The numerical solution for equation 12 can be solved by a variation of the Nicholson and Olmstead method[6]

$$\Psi_m = \left(k^0\tau - \frac{k^0\tau}{2L}\sum_{i=1}^{m}\Psi_i\right)e^{-\alpha\phi} - \frac{k^0\tau}{2L}\sum_{i=1}^{m}\Psi_i e^{(1-\alpha)\phi} \tag{13}$$

Separating the first term in the summation yields

$$\Psi_m + \frac{k^0\tau}{2L}\Psi_m e^{-\alpha\phi} + \frac{k^o\tau}{2L}\Psi_m e^{(1-\alpha)\phi} = \left(k^0\tau - \frac{k^0\tau}{2L}\sum_{i=1}^{m-1}\Psi_i\right)e^{-\alpha\phi} - \frac{k^0\tau}{2L}\sum_{i=1}^{m-1}\Psi_i e^{(1-\alpha)\phi} \quad (14)$$

Solving for Ψ_m yields

$$\Psi_m = \frac{\left(k^0\tau - \frac{k^0\tau}{2L}\sum_{i=1}^{m-1}\Psi_i\right)e^{-\alpha\phi} - \frac{k^0\tau}{2L}\sum_{i=1}^{m-1}\Psi_i e^{(1-\alpha)\phi}}{1 + \frac{k^0\tau}{2L}e^{-\alpha\phi} + \frac{k^0\tau}{2L}e^{(1-\alpha)\phi}} \quad (15)$$

Computation of theoretical voltammograms was done in MATLAB using the equation above.

At the request of the reviewers, we add the following commentary to clarify our waveform, the method in which we calculate currents, and how our calculated values compare with previous simulations by others. The generalized potential waveform used in the simulation is presented in Figure S-25.

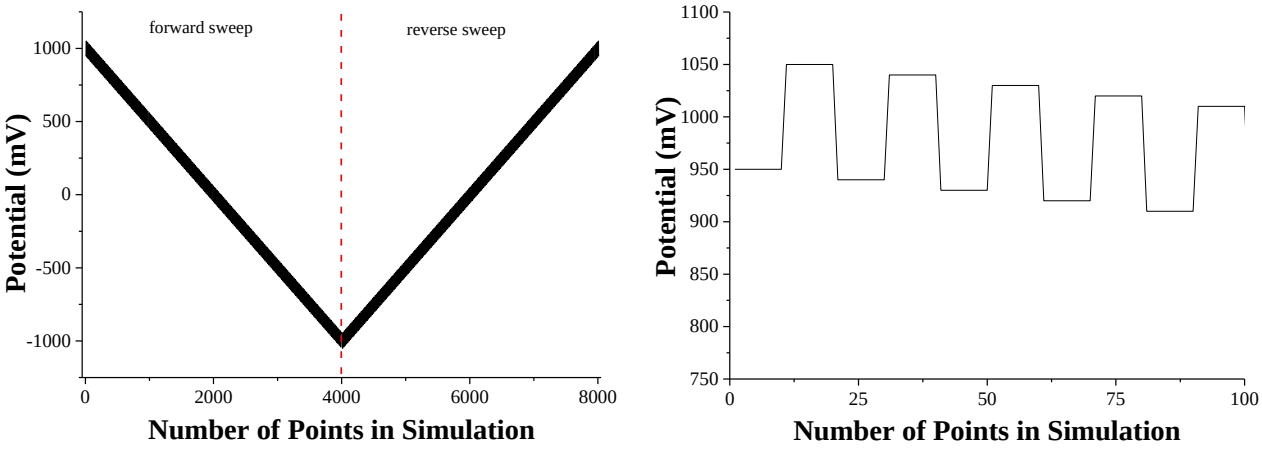

Figure S-25. Potential waveform used in this simulation. A zoom of the initial steps is shown in the panel on right.

The initial potential in all simulations was 1000 mV relative to E^0 = 0 mV. The potential stepped negatively to -1000 mV before returning to the initial potential. At this initial potential, only Ox is present at the electrode surface. The number of discrete potentials spanning the 4000 mV range from the initial potential to the switching potential (and back) is determined by the increment times the number of square wave pulses per period. For example, when 10 mV was chosen as the increment, the number of discrete potential steps is 800. The number of discrete current values computed was determined by the number of iterations, L, on each potential pulse.

For example, L = 10, the number of currents computed is 8000. [1] The panel on right in Figure S-25 is similar to Figure 7.3.13 on page 294 of Bard and Faulkner.[7] Our simulations begin at 1000 mV, then 950 mV, then 1050 mV, then 940 mV, then 1040 mV, and so forth. The "downward" pulses can also be called the "forward" pulses and correspond to the cathodic processes. Similarly, "upward" pulses are "reverse" pulses corresponding to anodic processes. Note: the plotting convention used herein treats reduction currents as positive and oxidative currents as negative values. Consequently, the net currents on the cathodic sweep, $\Delta\Psi_f^s$, are positive currents and the net currents on the anodic sweep, $\Delta\Psi_r^s$, are negative currents.

The calculated currents associated with each and every pulse in Figure S-25 are shown in Figure S-26. This figure is identical in shape to Figure 7.3.14 in Bard and Faulkner[7] and in Figure 2 of Osteryoung and O'Dea.[8]

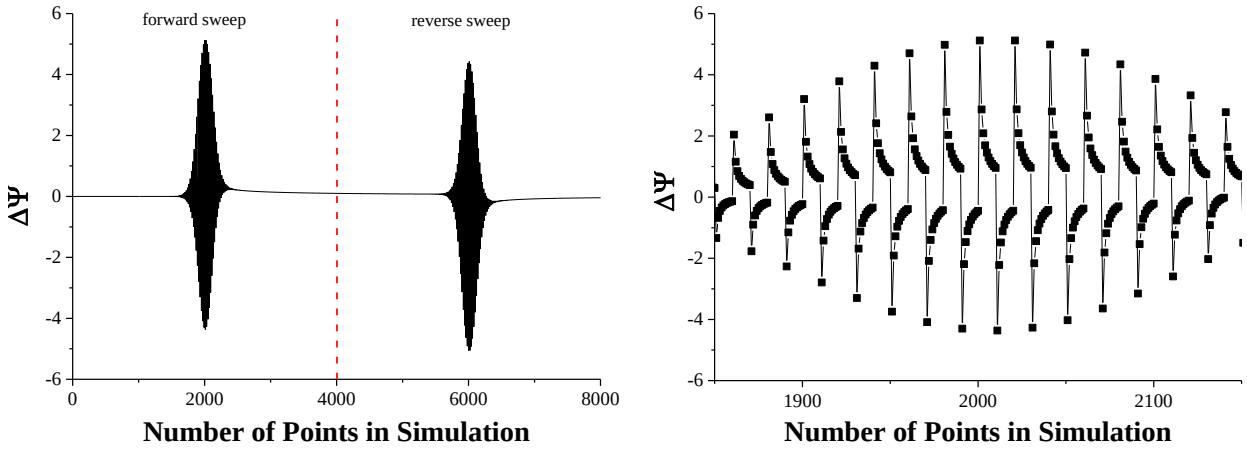

Figure S-26. The calculated currents as a function of potential versus the number of points in the simulation are shown for a reversible, diffusional process when n = 1. The panel on right is a zoom of calculated currents near E^0.

Our numerical approximation to the current integral is a recursive calculation. All previous values of the current are incorporated into the calculation of the next value. The current at the end of each potential pulse are the individual currents and used to compute the difference current as a function of potential (see Figure S-27).

[1] This value is actually 8020 because of the manner in which Pine adds an extra "turn around" set of pulses in their waveform which we mimic to be as close to experimental conditions as possible.

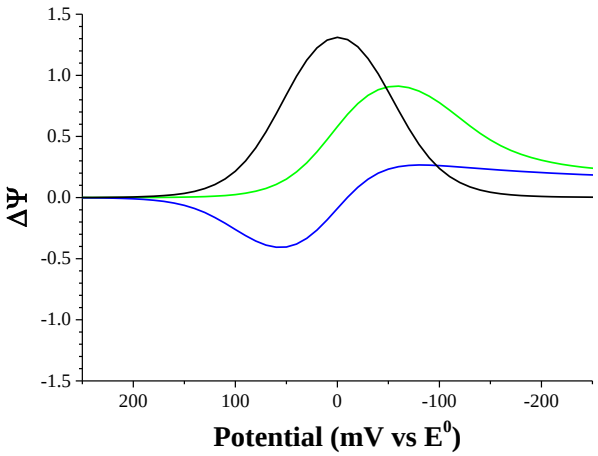

Figure S-27. The individual dimensionless currents forward (green), reverse (blue), and the net current (black) for the forward sweep corresponding to Figure S-26.

Note that in Figure S-27, we have only plotted our forward sweep (1000 mV to -1000 mV, zoomed in on the potential axis) so that the representation is identical to that in Figure 7.13.15 in Bard and Faulkner[7] and Figure 3 in Osteryoung and O'Dea.[8] We compute the average potentials and difference currents in exactly the same manner expressed in these two texts. Thus our simulations are carried out in the proper format of O'Dea, Osteryoung, and Osteryoung.[8-12] In the early publications by O'Dea, Osteryoung, and Osteryoung, $\Delta\Psi = 1.311$ for the reversible, diffusional process when pulse height = 50 mV and step height = 10 mV.[9,10] In subsequent publications, and in the table found in Bard and Faulkner[7] and O'Dea and Osteryoung,[8] $\Delta\Psi = 0.9281$ for the same pulse height and step height. We find this difference in peak magnitude interesting and note that $\frac{1.311}{0.9281} = 1.4125$. This closely compares with $\sqrt{2} = 1.4142$. This led us to investigate why early Osteryoung reports[9,10] differ in values from later reports.[8,11-12] It seems as though the Osteryoungs changed their definition of d, the discrete time after each potential step – a value that was adapted from Nicholson and Olmstead.[6] The early Osteryoung reports define τ to be the period of the wave, *i.e.*, the time for both a down and up pulse pair. The later reports define τ as just the time of one pulse. Thus $d = \frac{\tau}{2L}$ in early reports and $d = \frac{\tau}{L}$ in later reports. When d is inserted into the evaluation of $S_k = 2\sqrt{d}\left(\sqrt{k} - \sqrt{k-1}\right)$ as directed by Nicholson and Olmstead, the final equation differs by a factor of $\sqrt{2}$. Our work is consistent with the early formulation of τ (and subsequently d). Though not directly published in either of our previous works, we do obtain $\Delta\Psi = 1.311$ as shown in Figure S-28 taken directly from MATLAB. Thus, our value of $\Delta\Psi$ is in perfect agreement with early Osteryoung work.

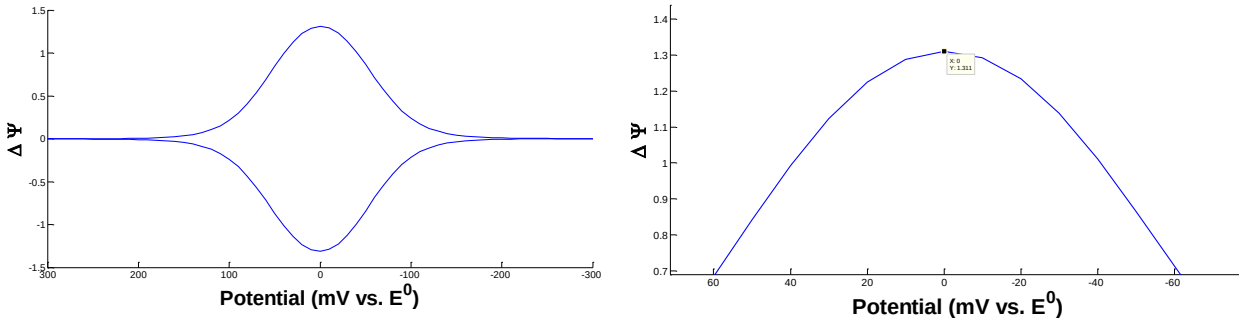

Figure S-28. Voltammogram of the reversible, diffusional process simulated in MATLAB for pulse height = 50 mV, step height = 10 mV, and L = 10. Note that the full range in potentials is not shown in either panel. The left panel is zoomed in on the x-axis and shows net currents on both the formal and reverse sweep. The right panel is zoomed in on both the x and y-axis to show only the forward net current.

Further comparison of the magnitudes of the difference current resulting from the potential pulses can be compared to the work by Mirčeski et al.[1] Mirčeski reports $\Delta\Psi_p$ values as a function of nE_{SW} in Table 2.1 of his book. If we use Mirčeski's step height of 2 mV and a pulse height of 50 mV, we obtain $\Delta\Psi_p = 1.2898$ compared to $\Delta\Psi_p = 0.7383$. Again, upon inspection, $\frac{1.2989}{0.7383} = 1.7469 \approx \sqrt{\pi} = 1.7724$. These values are within round off error and probably result from the number of subintervals used to calculate the value. Mirčeski defines his dimensionless current in equation 2.1 on page 14 of his text (included in Figure 8). Mann, Helfick, and Bottomley define the dimensionless current for a diffusional process as

$$i(t) = \Psi(t) nFA\sqrt{D_{Ox}}\frac{C^*_{Ox}}{\sqrt{\pi\tau}} = \frac{\Psi(t)\sqrt{D_{Ox}}C^*_{Ox}}{H\pi\sqrt{\tau}}$$

(Eq. 38 in the SI for Mann, Helfrick, and Bottomley). The Bottomley group and the Osteryoung group both use the Cottrell equation to convert current in SI units to a dimensionless current. However, Mirčeski uses the aforementioned equation to do such a conversion. The difference in these two equations is in fact the $\sqrt{\pi}$, which is a constant. Thus, the dimensionless current values from this work are in excellent agreement with those published by Mirčeski et al.

The recursive calculation of current on each step for every step in the voltammogram was performed by systematic variation over the following intervals: 1 ms $\leq \tau \leq$ 5 s, 10 mV $\leq E_{sw} \leq$ 90 mV, 1 mV $\leq \delta E \leq$ 25 mV, 0 mV $\leq E_\lambda \leq$ 1000 mV, and L = 20 over each period. Specific values of each parameter are given in the following table.

Empirical Parameters	Range	When held constant
Period, τ, in ms	1, 2, 5, 10, 20, 50, 100, 200, 500, 1000, 2000, 5000	50
Increment, δE, in mV	1, 3, 5, 7, 9, 11, 13, 15, 17, 19, 21, 23, 25	10
Amplitude, E_{SW} in mV	10, 20, 30, 40, 50, 60, 70, 80, 90	50

Period limits were set in consideration of typical potentiostat rise times, commonly encountered solution resistances and electrode double layer capacitances as well as the time duration required per scan. Increment limits were set in consideration of the number of points to define the peak. An increment of 1 mV maximizes the number of points to define the peak at the expense of a significantly longer time of experiment. The uncertainty in peak potential measurements increases with increment. Amplitude limits were set in accordance with the range typically used in SWV. Peak currents and widths are proportional to amplitude.

Simulations were also conducted over the range in $-6 \leq \log k^0 \leq 2$. These limits encompass the range historically associated with an irreversible and reversible process.

References

(1) Mirčeski, V.; Komorsky-Lovrić, Š.; Lovrić, M. *Square Wave Voltammetry: Theory and Application*; Springer-Verlag: Berlin, 2007.

(2) O'Dea, J. J.; Osteryoung, J. G. *Anal. Chem.* **1993**, *65*, 3090.

(3) Reeves, J. H.; Song, S.; Bowden, E. F. *Anal. Chem.* **1993**, *65*, 683.

(4) Mirčeski, V.; Lovrić, M. *Electroanalysis* **1997**, *9*, 1283.

(5) Mirčeski, V.; Laborda, E.; Guziejewski, D.; Compton, R. G. *Anal. Chem.* **2013**, *85*, 5586.

(6) Nicholson, R. S.; Olmstead, M. L. In *Electrochemistry: Calculations, Simulation and Instrumentation,*; Mattson, J. S., Marks, H. B., MacDonald, H. C., Eds.; Marcel Dekker: New York, 1972; Vol. 2, Ch. 5.

(7) Bard, A. J.; Faulkner, L. R. *Electrochemical Methods: Fundamentals and Applications*; 2nd ed.; Wiley: New York, 2000.

(8) Osteryoung, J. G.; O'Dea, J. J. In *Electroanalytical chemistry: a series of advances*; Bard, A. J., Ed.; Marcel Dekker, Inc: New York, 1986; Vol. 14, p 209.

(9) O'Dea, J. J., *Ph.D. Dissertation*, Colorado State University, 1979.

(10) O'Dea, J. J.; Osteryoung, J.; Osteryoung, R. A. *Anal. Chem.* **1981**, *53*, 695.

(11) O'Dea, J. J.; Osteryoung, J.; Osteryoung, R. A. *J. Phys. Chem.* **1983**, *87*, 3911.

(12) Osteryoung, J. G.; Osteryoung, R. A. *Anal. Chem.* **1985**, *57*, 101A.